Plasma instabilities in cross-field configuration: an analysis of the relevance of different modes for electron transport

IEPC-2019-758

Presented at the 36th International Electric Propulsion Conference
University of Vienna, Austria
September 15-20, 2019

Sedina Tsikata*
ICARE, CNRS UPR 3021, 1C ave de la Recherche Scientifique, 45071 Orléans, France

and

Kentaro Hara†
Stanford University, Stanford, California, 94305, USA
Texas A&M University, College Station, Texas, 77845, USA

Over the past several years, an increasing number of instabilities have been studied in the crossed field discharge of Hall thrusters in experiments and simulations. These oscillations cover a range of ionization- and drift-driven instabilities, and appear to influence global discharge features, such as the localization of the ionization region. They are also believed to play a role in subtle aspects such as anomalous electron transport, whose understanding is key to developing predictive codes. This paper draws on recent experimental insights to better analyze the conditions under which different instabilities possibly relevant to transport in the thruster may arise.

I. Introduction

A combination of theoretical analysis, numerical simulations and experiments has allowed the study of a range of instabilities in Hall thrusters in recent years. A number of these instabilities have been characterized as ionization-driven phenomena, such as the breathing mode,[1,2] ion transit time oscillations[3] and spokes.[4] Instabilities such as the electron cyclotron drift instability (ECDI)[5] and other instabilities[6] have been shown to be excited by the fast azimuthal electron drift established by the axial electric field and radial magnetic field configuration of thrusters. Far from merely reflecting ionization features of the discharge, these instabilities may contribute to the anomalous electron current observed in thrusters[7–10] and other devices.[11] Other instabilities affect thruster operation in different ways, such as ion acoustic turbulence, identified in hollow cathode plasmas and implicated in cathode erosion.[12] Conditions for the appearance of the modified two-stream instability in thrusters have also been recently investigated,[13] and a number of fluid instabilities were also studied early on,[14] although their link to the discharge characteristics remains unclear.

Establishing a definitive link between a particular instability and global observed features of the discharge, such as the level of electron current, is complicated by different factors, including the likely non-linear coupling between waves of different length scales and frequencies and the lack of diagnostic capability and access to study instabilities experimentally. In particular, where anomalous electron transport is concerned, although numerical evidence points to the role of the ECDI, there is no basis yet to exclude contributions from other

*Researcher, Electric Propulsion Team, sedina.tsikata@cnrs-orleans.fr
†Assistant Professor, Aeronautics and Astronautics, kenhara@stanford.edu

instabilities. It is therefore worth trying to establish more clearly (i) which instabilities are susceptible to being excited in different thruster operating regimes, (ii) whether a relative idea of their contributions to transport can be established across these regimes, and (iii) how studies which account for competing phenomena (such as the ECDI and modified two-stream instability (MTSI) in space plasmas[15]) can assist in the analysis of anomalous transport in thrusters.

In this contribution, an evaluation of the relevance of different instabilities in transport across different operating regimes is made using information available from experimental measurements (coherent,[16] incoherent Thomson scattering), and PIC simulations (using a code similar to the PIC code developed in JAXA[17]).

II. Experimental methods involved

A. Overview

Thomson scattering is a powerful tool for the study of instabilities and electron properties. It involves the scattering of electromagnetic radiation on free charges in a plasma, and is distinguished by two regimes of observation. In the incoherent scattering regime, an observation length scale below the electron Debye length is examined, giving access to spectra reflecting the individual thermal fluctuations of the main scatterers (electrons) and thus allowing the electron energy distribution function, density, and even drift velocity to deduced from the scattered spectra.

The coherent (or collective) scattering regime is that for which length scales larger that the electron Debye length are probed. At these length scales, the scattered spectra reflect the collective movements of electrons. Such collective motions are characteristic of self-organization in the plasma due to the presence of plasma waves. Tuning the observation length scale to that of this plasma organization allows the detection and study of waves such as the electron cyclotron instability, inaccessible to other diagnostic methods in the thruster plasma plasmas.

B. Coherent Thomson scattering for studies of instabilities at small scales

The experimental implementation of coherent Thomson scattering (CTS) for thruster studies has been accomplished over the past decade with a diagnostic we have developed known as PRAXIS.[16,22] This diagnostic has extremely high sensitivity and enables measurements of electron density fluctuations at the millimeter scale. We have previously estimated the density fluctuation rate to be about 1% of the mean density.

The diagnostic uses a monomode, continuous CO_2 laser of 10.6 μm wavelength and about 40 W power. The diagnostic observation wave vector $\vec{k}$ is defined by the Bragg relation: $\vec{k} = \vec{k_s} - \vec{k_i}$, where $\vec{k_s}$ is the scattering wave vector and $\vec{k_i}$ the incident wave vector. Two beams are used to define the observation wave vector and to recover scattered radiation. A low-intensity local oscillator beam, frequency-upshifted by 60 MHz with respect to the initial laser frequency, is and mixed with the plasma-scattered radiation. This heterodyne scheme allows signal detection not around the initial laser frequency, but in the more accessible MHz range. The signal recovered is demodulated to recover the pure scattered signal information. The second beam, a high intensity primary beam formed from most of the incident laser power, provides a high-amplitude incident field for scattering in the measurement volume. This beam is not transmitted to the detector, but dumped onto an absorber after it has been transmitted across the plasma. The overlap of the two beams in the plasma forms the observation volume, which in our experiments typically traverses the entire thruster diameter.

In these experiments, a range of measurements can be accessed by taking advantage of the variable wave vector magnitude and orientation offered by our setup. A change to the wave vector magnitude (accomplished using a series of mirrors mounted on the bench which can adapt the separation between the local oscillator and primary beams) allows the wave frequency to be tracked across at different observation length scales, giving access to the experimentally-measured dispersion relation. A modification of the wave vector orientation allows wave propagation in two planes different planes to be examined: the $(\vec{E} \times \vec{B}, \vec{E})$ plane and the $(\vec{E} \times \vec{B}, \vec{B})$ plane. This has been used to produce experimental evidence for propagation of the ECDI in three dimensions in the Hall thruster.[23]

In order to fully interpret the wave behavior, aside from the dispersion relation, we also examine the density fluctuation amplitude. The normalized scattering spectra provide a measure of the density fluctuation over the spectral frequency range, $S(k, \omega)$. The dynamic form factor signal, integrated over the frequency range in which the signal appears, gives the unitless "static form factor", $S(k)$, used in subsequent discussions to describe the density fluctuation intensity.

C. Incoherent Thomson scattering for studies of electron properties

The information gained from CTS has been essential to the detection and characterization of instabilities: not only the ECDI, but also an axially-propagating instability described in later work.[24] Yet full interpretation of the significance of the results obtained to date should incorporate not only characterization of the density fluctuations present in the plume, but also the corresponding local electron property information in the regions where instabilities are identified. For this reason, the development of a complementary incoherent Thomson scattering (ITS) diagnostic has been a priority.

This has been recently achieved with the design and construction of a new ITS bench known as THETIS. Like PRAXIS, this diagnostic is distinguished by its high sensitivity: we have demonstrated that it gives access to electron property information in plasmas with densities as low as 10^{16} /m^3. This opens up the possibility to studies of a range of magnetized and unmagnetized plasma sources, including thrusters.

This diagnostic uses a different incident electromagnetic radiation source (a frequency-doubled 532 nm Nd:YAG laser operating at 10 Hz and with nominal pulse energy of 430 mJ). Full details on the main diagnostic features have been provided in a recent publication.[25] Fig. 1 shows a simplified representation of the scattering configurations used for the two diagnostics.

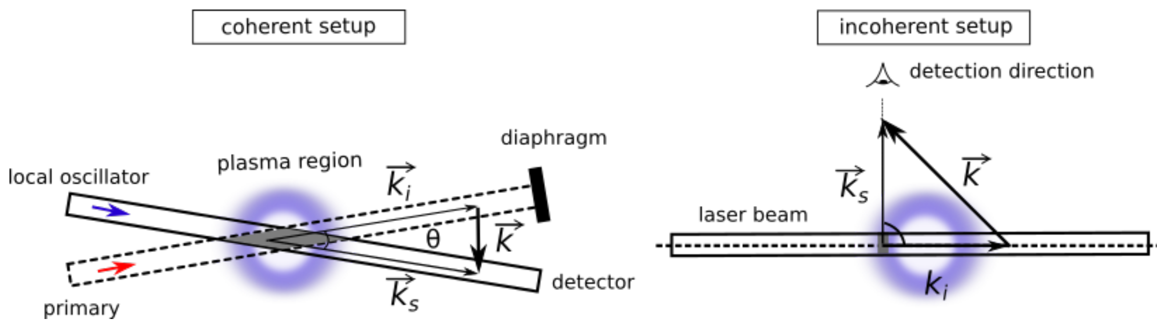

Figure 1: Scattering configurations employed for coherent and incoherent Thomson scattering in the experimental investigations used relevant to this work

III. Kinetic dispersion relation

Various types of linear dispersion relation (fluid and kinetic) can be derived by from the Vlasov-Poisson system.

A. Linear perturbation theory

The Poisson equation is given by

$$\nabla^2\phi = -\frac{e}{\epsilon_0}(n_i - n_e), \tag{1}$$

where ϕ is the electrostatic potential, e is the elementary charge, ϵ_0 is the permittivity, n_i is the ion density, and n_e is the electron density. Here we will assume a linear perturbation on each quantity, e.g. for arbitrary parameter $Q = Q_0 + Q_1 \exp[i(\vec{k}\cdot\vec{x} - \omega t]$, where subscripts 0 and 1 denote the equilibrium and perturbation quantities, $\vec{k}$ is the wavevector, $\vec{x}$ is the position, ω is the wave frequency, and t is time. Then, the perturbed Poisson equation can be written as

$$k^2\phi_1 = \frac{e}{\epsilon_0}(n_{i,1} - n_{e,1}), \tag{2}$$

where ϕ_1 is the perturbed potential and $k^2 = |\vec{k}|^2$.

For the electrons, the Vlasov equation is given by

$$\frac{\partial f}{\partial t} + \vec{v}\cdot\frac{\partial f}{\partial \vec{v}} - \frac{e}{m_e}\left(\vec{E} + \vec{v}\times\vec{B}\right)\cdot\frac{\partial f}{\partial \vec{v}} = \frac{\delta f}{\delta t}, \tag{3}$$

where $f(\vec{x}, \vec{v}, t)$ is the velocity distribution function (VDF), m_e is the electron mass, $\vec{v}$ is the particle velocity, $\vec{E}$ is the electric field and $\vec{B}$ is the magnetic field, and the right hand side is the collision term. We consider the dynamics along and across the magnetic field to be denoted by $\|$ and $\perp$, respectively. Assuming an isotropic Maxwellian distribution function for the equilibrium component of f, the perturbed electron density can be written as,

$$n_{e,1} = \frac{e}{m_e}\frac{n_0\phi_1}{v_{th,e}^2}\left\{1 + \frac{\omega}{a}\left[Z\left(\frac{\omega}{a}\right)I_0(b)\exp(-b) + \sum_{n=1}^{\infty}\left\{Z\left(\frac{\omega+n\Omega}{a}\right) + Z\left(\frac{\omega-n\Omega}{a}\right)\right\}I_n(b)\exp(-b),\right]\right\} \tag{4}$$

where $a = \sqrt{2}k_{\|}v_{th,e}$, $Z(\xi) = \pi^{-1/2}\int\frac{\exp(-s)}{s-\xi}ds$ is the plasma dispersion relation, $b = (k_\perp v_{th,e}/\omega_B)^2 = (k_\perp r_{L,e})^2$, $v_{th,e}$ is the electron thermal speed, $\omega_B = eB/m_e$ is the Larmor radius, and I_n is the n-th modified Bessel function of the first kind. Note that the plasma dispersion relation satisfies $Z' = -2(1+\xi Z)$.

For the ions, the continuity and momentum equations are considered. If the ions are assumed to be cold, the perturbed ion density can be written as

$$n_{i,1} = \frac{e}{m_i}\frac{n_0\phi_1 k^2}{(\omega - \vec{k}\cdot\vec{v}_0)^2 + \nu_{\text{ion}}^2}, \tag{5}$$

where m_i is the ion mass, v_0 is the ion drift, and ν_{ion} is the ionization frequency. If the ions are not cold and no ionization occurs,

$$n_{i,1} = \frac{1}{2}\frac{e}{m_i}\frac{n_0\phi_1}{v_{th,i}^2}Z'\left(\frac{\omega - \vec{k}\cdot\vec{v}_0}{\sqrt{2}kv_{th,i}}\right), \tag{6}$$

where $v_{th,i}$ is the ion thermal speed. By combining the perturbed potential (Eq. 2), perturbed electron density (Eq. 4), and perturbed ion density (Eq. 5 for cold ions and Eq. 6 for warm ions without ionization), various types of linear dispersion relations can be derived. Also note that electron guiding center motion is not accounted for in Eq. 4 so the electron drift can be considered via the ion drift since it is merely a relative motion between the ions and electrons.

B. Electron cyclotron drift instability (ECDI)

The dispersion relation for ECDI has been discussed by Ducrocq,[18] Tsikata,[11] Cavalier.[19] Here, the main assumptions are that (i) the $E\times B$ drift is in the y direction ($\omega - k_yV_d$, where V_d is the drift), (ii) ions are cold ($T_i = 0$), and (iii) no ionization. The three-dimensional (3D) dispersion relation can be then written as,[18]

$$k^2\lambda_D^2\left(1 - \frac{m_e}{m_i}\frac{\omega_{pe}^2}{\omega^2}\right) + 1 + \bar{\xi}\left\{Z(\bar{\xi})I_0(b)\exp(-b) + \sum_{n=1}^{\infty}\left[Z\left(\xi^+\right) + Z(\xi^-)\right]I_n(b)\exp(-b)\right\} = 0, \tag{7}$$

where

$$\xi^\pm = \frac{\omega - k_yV_d \pm n\Omega}{\sqrt{2}k_{\|}v_{th,e}}, \tag{8}$$

λ_D is the Debye length, ω_{pe} is the electron plasma frequency, and $\bar{\xi} = (\xi^+ + \xi^-)/2$. Note that if $k_{\|} = 0$, then the dispersion relation becomes 2D. One can assume $\xi \to \infty$.

$$k_\perp^2\lambda_D^2\left(1 - \frac{m_e}{m_i}\frac{\omega_{pe}^2}{\omega^2}\right) + 1 - I_0(b)\exp(-b) + \sum_{n=1}^{\infty}\frac{2(\omega - k_yV_d)^2 I_n(b)\exp(-b))}{(n\omega_B)^2 - (\omega - k_yV_d)^2} = 0. \tag{9}$$

Figure 2 shows the results of the ECDI dispersion relation, as discussed in Eq. 7. Here, the ion species is xenon, $v_{th,e}/V_d = 5.304$, $v_{th,i}/v_{th,e} = 2\times10^{-4}$, and no ion drift in the cross-field direction are assumed. It can be seen that the parallel dynamics influences the ECDI: when $k_{\|}\to 0$ (large wavelength), the dispersion relation shows a more resonant-lick structure. The peak at $k_y\lambda_D \approx 1.04$ agrees with $k_y = \omega_B/V_d$, which is the resonance in Eq. 9. The phase velocity of the waves is approximately the ion acoustic speed for the 2D dispersion relation, while it can be seen that the waves for large wavelength modes (small k_y) in the 3D solution has a larger phase velocity than the ion acoustic speed, which means that the effects of the waves on ion dynamics are fluid type more than kinetic.

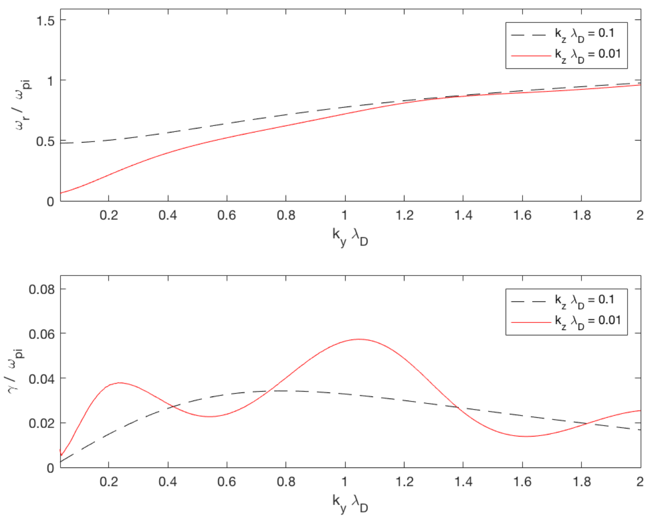

Figure 2: ECDI theory: The real frequency and growth rate for $k_x = 0$ and two $k_z = k_{\|}$ values. Small k_z corresponds to a 2D like resonance while a larger k_z corresponds to an ion acoustic type instability (3D).

IV. The electron cyclotron drift instability field amplitude, revisited

In order to gauge the contribution of the ECDI to the overall electron transport, it is necessary to know its amplitude, which simulations show can be as much as a quarter of the applied electric field.[8] In the past, we have combined measurements of the density fluctuations from coherent scattering with some assumptions on the local plasma state. Revisions to this calculation can now be made on the basis of (i) additional experiments performed on small thrusters using coherent Thomson scattering, and (ii) recent measurements of electron properties in small thrusters using incoherent Thomson scattering.

The following observations allow for a re-estimation of the ECDI field:

- **Density fluctuation observations on thrusters in the 200 W range**: on small thrusters, similar features for the ECDI that were first measured on a 5 kW thruster were identified (frequency range and fluctuation intensity. This observation suggests not only universality of the presence ECDI across different architectures and thruster sizes, but also its amplitude.
- **Electron properties in thrusters in the 200 W range**: the electron temperature which assumed in the region where the ECDI was measured in previous work was about 20 eV. With new ITS measurements, electron temperatures higher than expected have been directly measured, in the region of 40 eV or higher. Similar measurements also allow us to revise the electron density lower, from an initial guess of 10^{17} - $10^{18}/\mathrm{m}^3$ down to only a few $10^{16}/\mathrm{m}^3$.

The form factor dependency on wavenumber has been shown[23] to be an exponential: $S(k) = S_0 e^{-bk}$, for which the amplitude S_0 was determined to be on the order of 10^6, and the parameter b, a characteristic scaling length, to be a few 10^{-4}.

Based on the following features deduced from experiments:

- the angle of main mode propagation in the $(\vec{E} \times \vec{B}, \vec{E})$ plane (the instability propagates outside the thruster due to convection, but in this plane points 10° towards the exit plane)
- and the $(\vec{E} \times \vec{B}, \vec{B})$ plane (the instability, rather than being aligned perpendicular to B, possesses a small component aligned with the magnetic field)

the density fluctuation rate is written

$$\langle \tilde{n}^2 \rangle \approx \frac{S_0 n_0}{(2\pi)^3} \int_0^\infty e^{-kb} dk \int ke^{-\frac{(\alpha-\mu_\alpha)^2}{2\sigma_\alpha{}^2}} d\alpha k \Delta\beta \tag{10}$$

where σ_α is 0.05 rad, the experimentally-determined angular opening of the mode in the $(\vec{E} \times \vec{B}, \vec{E})$ plane, and μ_α is the angular location of the largest amplitude mode in the $(\vec{E} \times \vec{B}, \vec{E})$ plane. β is 0.08 rad and the peak width $\Delta\beta$ is about 0.15 rad.

Using data available from experiments on a 200 W thruster, this equation gives the mean square density fluctuation of $\langle \tilde{n}^2 \rangle \approx 0.30 \times 10^{31}$ m^{-6} and an r.m.s density fluctuation value of 1.74×10^{15} m^{-3}.

Now, based on an experimentally-determined local density of 2×10^{16} in the same region where the instability has been measured, on a small thruster, we find the density fluctuation rate

$$\frac{\sqrt{\langle \tilde{n}^2 \rangle}}{n_0} = 0.0872 \tag{11}$$

This is a density fluctuation rate of 8.7%, several times larger than what we estimated in past work using assumptions on the local plasma state. Experiments on a larger thruster, to take place in the near future, will be necessary to provide a clearer evaluation of past data. But the current finding is clear evidence of the importance of complementary ITS measurements, not only to understanding discharge features, but to establishing properties of modes in order to calculate their contribution to transport.

We can now use this information, along with the local electron properties, to estimate the fluctuation-induced field more accurately.

The expression relating the local density fluctuation to the potential is $\frac{\tilde{n}}{n_0} = \frac{\phi e}{k_B T_e}$. From the local electron temperature, now revised upwards from as estimation of 20 eV up to about 40 eV, and with the newly-determined density fluctuation rate of 8.7%, we can find a value of potential of 3.48 V. This potential associated with this instability is expressed over a length scale on the order of a millimeter (i.e., the observation length scale of the experiment), giving an electric field value of 3.48×10^3 V/m. This large value is in line with magnitudes expected from PIC numerical simulations performed by Adam and Héron,[8] for an accelerating electric field of amplitude on the order of 10^4 V/m.

A. Modified two-stream instability (MTSI)

Another type of cross-field instability mechanism has been proposed by McBride and Ott[20] and others.[21] Here the main assumptions are that (i) ion drift is considered in all directions, (ii) ions are warm ($T_i \neq 0$), (iii) ionizations are not accounted for, and (iv) most importantly, the kinetic resonances are negligible, i.e. $k_\perp r_{L,e} = \sqrt{b} \ll 1$. The modified Bessel function of the first kind behaves as $I_n(b)\exp(-b) \to 0$ for $n > 1$ for $b \to 0$, while $I_{n=1}(0) = 1$. Therefore, Eq. 7 can be approximated as

$$k^2\lambda_D^2 \left[1 - \frac{1}{2}\frac{T_e}{T_i} Z'\left(\frac{\omega - \vec{k}\cdot\vec{U}}{\sqrt{2}k v_{th,i}}\right)\right] + 1 - I_0(b)\exp(-b)\left[1 + \frac{1}{2}Z'\left(\frac{\omega}{\sqrt{2}k_\parallel v_{th,e}}\right)\right]. \tag{12}$$

If one takes Eq. 13, and assume $k_\perp/k = \cos\theta$ and $k_\parallel/k = \sin\theta$ as well as small θ, the dispersion equation can be written as

$$1 - \frac{T_e}{T_i}\frac{1}{2\tilde{\kappa}^2} Z'\left[\sqrt{\frac{T_e}{T_i}}\frac{\tilde{\omega}}{\sqrt{2}\tilde{k}} - \frac{U}{\sqrt{2}v_{th,i}}\right] - \frac{1}{2\tilde{\kappa}^2} Z'\left(\frac{\tilde{\omega}}{\sqrt{2}\tilde{k}\tilde{\theta}}\right) = 0, \tag{13}$$

where $\tilde{\omega} = \omega/\omega_{pi}[1 + (\omega_{pe}^2/\omega_B^2)]^{1/2}$, $\tilde{\kappa} = (kr_{Le})(\omega_B/\omega_{pe})[1 + (\omega_{pe}^2/\omega_B^2)]^{1/2}$, and $\tilde{\theta} = \theta(m_i/m_e)^{1/2}$. The results of the MTSI theory (reproduced from Ref. 20) is shown in Fig. 3.

Let us make a few more assumptions, such as (i) no ion Landau damping: $|\omega - \vec{k}\cdot\vec{U}| \gg kv_{th,i}$, (ii) $k_\parallel v_{th,e} \ll |\omega|$, and (iii) $b = (k_\perp r_{L,e})^2 \ll 1$. Then, Eq. 13 can be written as

$$1 + \frac{k_\perp^2}{k^2}\frac{\omega_{pe}^2}{\omega_B^2} - \frac{\omega_{pi}^2}{(\omega - \vec{k}\cdot\vec{U})^2} - \frac{k_\parallel^2}{k^2}\frac{\omega_{pe}^2}{\omega^2} = 0, \tag{14}$$

which resembles a two-stream instability. Thus, it is called the "modified" two-stream instability. The last term suggest that the modified two-stream instability acts as if the electrons are heavier, i.e. $\tilde{m}_e = m_e k/k_\parallel$. Due to the MTSI, the electrons can be heated in the parallel direction and the ions can be heated in the perpendicular direction. In addition, if the gyrofrequency is smaller than the electron plasma frequency, the second term becomes larger, which is equivalent to the charge density being treated smaller. Hence, the modified two-stream instability could be less important when the electrons are less magnetized.

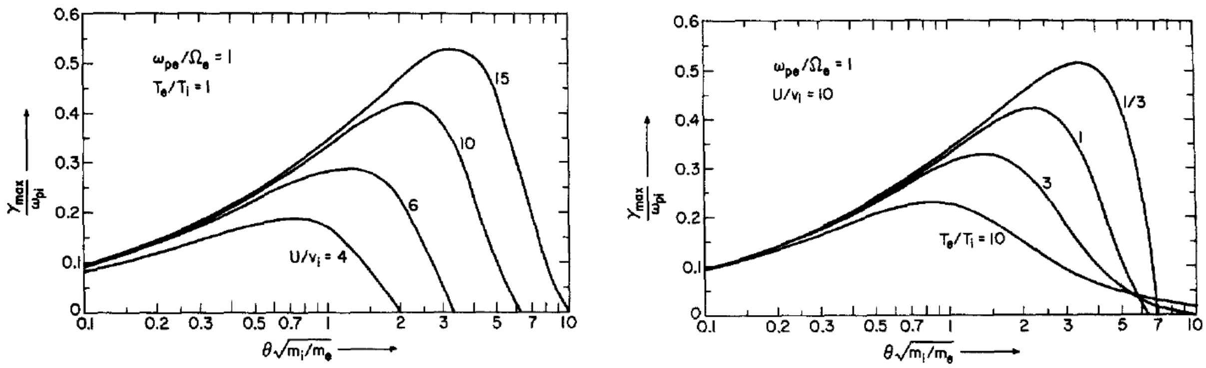

Figure 3: MTSI theory. Left: variation of drift velocity. Right: variation of electron-to-ion temperature ratio. Reproduced from Ref. 20.

B. The ion acoustic instability: gradient-induced modifications of the growth rate

In recent studies of the electron cyclotron drift instability, measured within a few millimeters of the thruster exit plane region in the acceleration region, we have pointed out similarities between the group velocity of the short-scale ECDI, directly measured by coherent Thomson scattering, to the group velocity expected for an ion acoustic mode, for which the group velocity is written $v_g = \sqrt{\frac{k_B T_e}{m_i}}$.

This initial observation is supported by considering two points: (i) the expected range of electron temperatures in the exit plane region, from simulations, and (ii) the fact that the ECDI has an ion acoustic limit. It should be emphasized that the similarity of the measured ECDI group velocity to an ion acoustic mode is not an an argument for a conversion between modes.

Experimental data on the electron properties can provide better clues regarding the features of the modes present in the acceleration region. This data has not previously been accessible, however, the development of a sensitive incoherent Thomson scattering diagnostic for the electron properties in this region now make this analysis tractable.

Regarding ion acoustic mode features, we note that the presence of electron temperature gradients in the region where the ECDI develops contributes significantly to the apparent growth rate of the ion acoustic mode. In the presence of such gradients,[21] the electron azimuthal drift is no longer v_d (E/B), but an effective drift velocity v_e,

$$v_e \to v_d + 1.5 \left(T_e^{-1} \frac{dT_e}{dx} \right) \left(\frac{T_e}{m_e \Omega_e} \right). \tag{15}$$

A negative gradient of a few eV per mm has been measured in the region where the ECDI is detected, conditions sufficient for a non-negligible modification of the drift velocity. This effect will be analyzed in detail once measurements on a larger thruster become available.

Other instabilities that may exist in the HETs include (i) Simon Hoh instability, (ii) gradient-drift instability, (iii) two-stream instabilities due to secondary electron emission, and (iv) current-carrying ion-acoustic instability from the cathode will also be analyzed in upcoming work.

V. Discussions about ECDI vs. MTSI

Using the SPT-100 results obtained by Cho's 2D full PIC simulation,[17] we attempt to evaluate which instabilities are large depending on the regions.

Figure 4 shows the colormap of ω_{pe}/ω_B. The electrons are weakly magnetized in all regions within the channel and downstream of the channel where the plasma exists. However, the plasma density becomes smaller in the wings of the plasma jet, while the magnetic field strength becomes larger near the pole pieces due to the design of the thruster. Near the region of the pole piece, $\omega_{pe} < \omega_B$. This indicates that the parallel heating of electrons may be largest near the region where $\omega_{pe} = \omega_B$.

The angle of the plasma flow, more precisely, plasma wave, with respect to the magnetic field angle also plays an important role in the dispersion relations. The ion flow streamline and the potential gradient

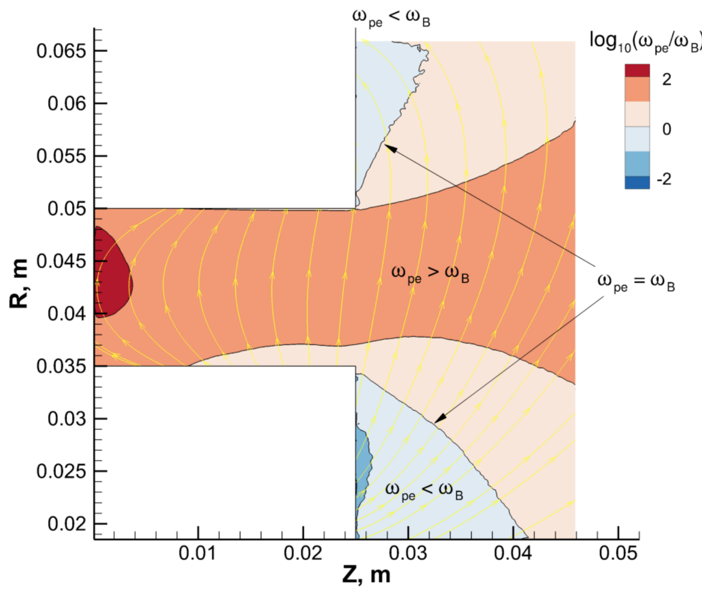

Figure 4: ω_{pe}/ω_B. The color map is for $\log_{10}(\omega_{pe}/\omega_B)$. The red shows the weakly magnetized region and the blue shows the more magnetized region.

are shown in Fig. 5(left) using orange line and light green line, respectively. The arrowed solid black line represents the magnetic field lines. The light green line is terminated near the cathode λ-line. The ion streamline shows a correlated axial beam in the channel center, while the ion divergence angle becomes larger as it goes off centerline. The ion streamline and the potential gradient overlaps well. The discrepancy comes potentially from the ionization term and some pressure term, since the agreement of the two indicates that $\vec{u}_i \propto \vec{E}$.

The angle can be represented as $k_\parallel/\sqrt{k_\parallel^2 + k_\perp^2} = \sin\alpha$. It was observed in the MTSI theory that $\alpha \approx 90°$ (with a correction of $\sqrt{m_e/m_i}$) gives the largest growth rate in a wide range of cases except when the drift velocity is large. Additionally, from the ECDI theory, $\alpha = 90°$ corresponds to $k_\parallel = 0$, which yields a more 2D like resonant dispersion solution. If $k_\parallel \neq 0$, then the dispersion relation becomes more 3D like, i.e. ion acoustic wave (see Fig. 2). The ion acoustic wave is more broadband, hence it is likely difficult to detect a resonant structure. This result shows that the ECDI resonance could be only observed in a limited region in the radial direction.

VI. Conclusions

This manuscript considers the features of multiple instabilities excited in the Hall thruster plasma. For the ECDI, the subject of several studies in the community, we revisit the main features of the dispersion relation and re-evaluate calculations of its electric field in light of new information available from experiments. These re-evaluations, based on more precise knowledge of the local electron properties where the ECDI has been detected, suggest a field amplitude compatible with simulation predictions by Adam and Héron. In light of recent work on the MTSI by Janhunen and colleagues, we perform simulations in order to determine what spatial localization may apply to both the ECDI and MTSI, and find that the ECDI resonances are sharply localized, a result not incompatible with experimental investigations, which have so far only detected smoothed resonances. Other instabilities will be analyzed in upcoming work.

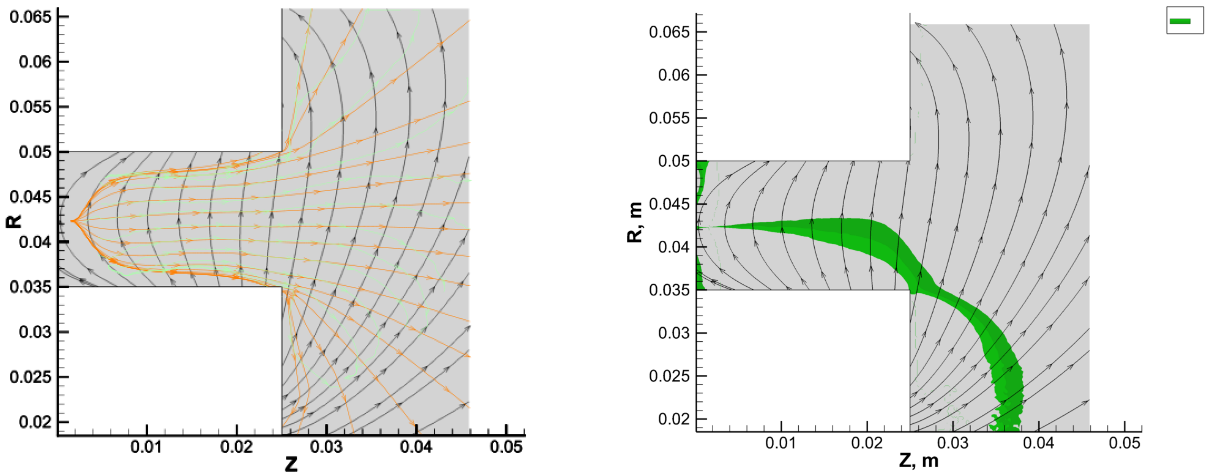

Figure 5: (Left) ion streamline (orange), potential gradient (light green), and magnetic field lines (black). (Right) The region where the ion flow is nearly perpendicular to the magnetic field lines, as can be seen from the orange and black line.

VII. Acknowledgments

The authors thank S. Cho for sharing the PIC simulation results for our discussion, B. Vincent for analysis of some ITS data and A. Héron for providing the code for the 3D ECDI theory. The second author acknowledges the support by the Air Force Office of Scientific Research under award number FA9550-18-1-0090 and by the US Department of Energy, Office of Science, Office of Fusion Energy Sciences under Award Number DE-SC0019045.

References

[1] J. P. Boeuf and L. Garrigues. *J. Appl. Phys.* **84**, 3541 (1998)

[2] K. Hara, M. J. Sekerak, A. D. Gallimore, I. D. Boyd, *J. Appl. Phys.* **115**, 203304 (2014)

[3] S. Barral, K. Makowski, Z. Peradzynski and M. Dudeck. *Phys. Plasmas* **12**, 073504 (2005)

[4] C. L. Ellison, Y. Raitses and N. J. Fisch, *Phys. Plasmas* **19**, 013503 (2012)

[5] D. W. Forslund, R. L. Morse and C. W. Nielson, *Phys. Rev. Lett.* **27**, 1424 (1971)

[6] A. Lazurenko, L. Albarde and A. Bouchoule, *Phys. Plasmas* **13**, 083503 (2006)

[7] J. W. Koo and I. D. Boyd, *Phys. Plasmas* **13**, No. 3 (2006)

[8] J. C. Adam, A. Heron, and G. Laval, *Phys. Plasmas* **11**, 295 (2004)

[9] M. Hirakawa, *25th International Electric Propulsion Conference*, IEPC-97-021, Worthington, OH, 1997

[10] T. Lafleur, S. Baalrud, and P. Chabert, *Phys. Plasmas* **23**, 053502 (2016).

[11] S. Tsikata and T. Minea, *Phys. Rev. Lett.* **114**, 185001 (2015)

[12] B. A. Jorns, I. Mikellides and D. Goebel, *Phys. Rev. E* **90**, 063106 (2014)

[13] S. Janhunen, A. Smolyakov, D. Sydorenko, M. Jimenez, I. Kaganovich, and Y. Raitses, *Phys. Plasmas* **25**, 082308 (2018)

[14] A. A. Litvak and N. J. Fisch, *Phys. Plasmas* **11**, 1379 (2004)

[15] L. Muschietti and B. Lembage, *J. Geophys. Res.: Space Phys.* **118**, 2267 (2013)

[16] S. Tsikata, N. Lemoine, V. Pisarev and D. Grésillon, *Phys. Plasmas* **16**, 033506 (2009)

[17] S. Cho, K. Komurasaki, and Y. Arakawa, *Phys. Plasmas* **20**, 063501 (2013)

[18] A Ducrocq, *Ph.D thesis, Ecole Polytechnique* (2006)

[19] J. Cavalier, N. Lemoine, B. Bonhomme, S. Tsikata, C. Honore, and G. Gresillon, *Phys. Plasmas* **20**, 082107 (2013)

[20] J. McBride, E. Ott, J. Boris, and J. Orens, *Phys. Fluids* **15**, 2367 (1972)

[21] N. Krall and P. Liewer, *Phys. Rev. A* **4**, 2094 (1971)

[22] S. Tsikata, PhD thesis, Ecole Polytechnique, France (2009)

[23] S. Tsikata, C. Honoré, N. Lemoine and D. M. Grésillon, *Phys. Plasmas* **17**, 112110 (2010)

[24] S. Tsikata, J. Cavalier, A. Héron, C. Honor N. Lemoine, D. Grésillon and D. Coulette, *Phys. Plasmas* **21** 072116 (2014)

[25] B. Vincent, S. Tsikata, S. Mazouffre, T. Minea and J. Fils, *P*lasma Sources Sci. Technol. **27**,055002 (2018)